Colloid Polym Sci 278:293–300 (2000)

ORIGINAL CONTRIBUTION

T. Ogasawara
K. Izawa
N. Hattori
H. Okabayashi
C.J. O'Connor

Growth process for fractal polymer aggregates formed by perfluorooctyltrimethoxysilane. Time-resolved small-angle X-ray scattering study

Received: 13 July 1999
Accepted in revised form: 6 October 1999

T. Ogasawara · K. Izawa · N. Hattori
H. Okabayashi (✉)
Department of Applied Chemistry
Nagoya Institute of Technology
Gokiso-cho, Showa-ku, Nagoya 466-855
Japan

C.J. O'Connor
Department of Chemistry
The University of Auckland
Private Bag 92019, Auckland, New Zealand

Abstract The acid-catalyzed condensation reaction of perfluorooctyltrimethoxysilane (PFOS) and *n*-octyltrimethoxysilane (OTMS) in ethanol has been followed by time-resolved synchrotron radiation small-angle X-ray scattering (SAXS) on a short time scale. SAXS curves for PFOS and OTMS have been interpreted as arising from mass fractals with $D_f = 2$ (PFOS) and $D_f = 1.7$ (OTMS). The time dependence of the apparent radius of gyration, obtained from the Guinier plots, showed that the growth of fractal precursors occurs in a two-step process within 2 h for PFOS and within 1.5 h for OTMS, in which small clusters involving monomers, dimers and trimers are formed in the initial step and formation of larger clusters occurs in the second step. Furthermore, it has been suggested that the hydrophobicity and lipophobicity of the bulky alkyl groups may also contribute to the formation of these giant aggregates.

Key words Perfluorooctyltrimethoxysilane · Mass fractal · Small-angle X-ray scattering

Introduction

The condensation reaction of alkoxides, such as tetramethylorthosilicate (TMOS) or tetraethylorthosilicate (TEOS), to yield a variety of silicas has often been used in sol–gel research. Bechtold [1] provided evidence that polymeric structures exist in silica solutions, while Sakka and Kamiya [2] demonstrated that silica fibers could be pulled from solution. Furthermore, Schaefer and Keefer [3] used small-angle X-ray scattering (SAXS) to elucidate the fractal characteristics of branched silica polymers. These investigations enforced reevaluation of the applicability of organic polymer concepts to silica solutions.

The emphasis in sol–gel research has been to find application in industrial areas such as coatings, aerogels [4] and others, and has been focussed on silicate precursors. Solution processing involves various intermediates or precursors which depend upon the reaction conditions. Elucidation of the nature of these precursors will lead to the development of various applications.

Fractal geometry [5], kinetic growth models [6–8] and small-angle-scattering (SAS) techniques [9–14] have all played a significant role in the elucidation of the intermediates or precursors which occur in solutions of TMOS or TEOS.

Brinker et al. [12] have examined the sol–gel transition in simple silicate systems (TEOS–alcohol–water systems with acid or base catalyst) using a SAXS technique. The results of the Guinier plots indicate that the size of the silicate clusters for the acid-catalyzed system do not vary over time, while for the base-catalyzed system the apparent radius of gyration of the largest molecules grew linearly during the time over which gelation occurred, i.e. from 20 Å 1.2 h after the addition of the base to 44 Å after 3.8 h.

Keefer [14] observed the evolution, on long time scales, of SAXS curves for fractally rough TEOS clusters

and from observation of the progressive steepening of the SAXS profiles was able to discuss the smoothing of the surface of the colloidal particles. However, very little is known about the time-resolved SAXS data within the initial time course (1 h) of the condensation reaction of alkoxide or alkylalkoxide.

Recently, Stellbrink et al. [15] used small-angle neutron scattering to investigate the self-assembling behavior of styryl-lithium head groups during the early stages of living anionic polymerization. The result showed that the scattering behavior can be analyzed in terms of a form factor for a mass fractal structure, as proposed by Beaucage and Schaefer [16].

Furthermore, alkylalkoxides [$R\mathrm{Si}(\mathrm{O}R')_3$, R = alkyl and R' = methyl or ethyl groups] have been used extensively to reinforce the interface between a fiber and a resin through chemical interaction with silane molecules [17–20]. For this particular reinforcement, the mechanism responsible for the improved adhesion has not yet been completely clarified, although many attempts to elucidate it have been carried out [21–26].

Of the many alkylalkoxides, perfluorooctyltrimethoxysilane (PFOS) is a representative of the silane coupling agents which can be used to control the wettability of the surface of materials. The microstructure of the PFOS layer, coated onto the surface of substrates, must play a critical role in the characteristic appearance of the surface. We may assume that the self-assembling behavior of the perfluorooctyl chains, in addition to that of the siloxane-polymer portions, exists in the polymerization process of the PFOS-substrate system, since the perfluorooctyl portion has both the characteristics of hydrophobicity and lipophobicity [27]. Thus, the self-assembling behavior of the PFOS chains must affect the microstructure of the PFOS layer.

In this present study, the polymerization process of PFOS in ethanolic solution was examined by use of time-resolved SAXS, in order to increase our understanding of the polymerization process of PFOS during the initial time course of the condensation reaction.

Experimental

Materials

1H,1H,2H,2H-PFOS [$\mathrm{F(CF_2)_6CH_2CH_2Si(OCH_3)_3}$] was purchased from Lancaster Synthesis, and *n*-octyltrimethoxysilane [$\mathrm{CH_3(CH_2)_6CH_2Si(OCH_3)_3}$, OTMS] was purchased from Fluka Chemical Company. These were used without further purification. An ethanol–water system was chosen as solvent and 1M HCl was used as a catalyst.

Gel permeation chromatography measurements

Values of M_n, M_w and M_w/M_n for the polymers obtained after phase-separation were estimated by gel permeation chromatography (GPC) using a TOSOH high-performance liquid chromatography system, which consists of a column oven (CO-8020) equipped with two GMHXL columns (60 cm each) in series, a solvent delivery pump (CCPS), a refractive index detector (RI-8020), and a UV detector (UV-8020). Tetrahydrofuran was used as the eluant at a flow rate of 1.0 ml/min. The chromatograms were calibrated with polystyrene standards.

^{1}H NMR measurements

^{1}H NMR spectra were recorded on a Varian XL-300 spectrometer operating at 300.112 MHz for protons (spectral width of 4500.5 Hz, 32 768 points in the time domain, acquisition time of 3.641 s and delay of 8.359 s). ^{1}H NMR measurements were made in 5-mm NMR sample tubes at 25.0 °C.

SAXS measurements

Time-resolved SAXS measurements were carried out by use of a synchrotron radiation X-ray scattering spectrometer (BL-10C) installed at the 2.5 GeV storage ring in the Photon Factory, Tsukuba, Japan, with SAS optics.

A one-dimensional position-sensitive proportional counter was used for detecting the scattering intensity. The wavelength of the radiation used was 1.488 Å, and the sample-to-detector distance was 65 cm. Slit corrections were not carried out because quasi-point-type optics were used. The details of the optics and instruments are given elsewhere [28]. Sample solutions were placed in a cell, fitted with a pair of mica windows with 1-mm path length, and held in a thermostatted cell holder maintained at 25.0 ± 0.1 °C by circulating water. Ten-minute SAXS measurements were repeated after appropriate time intervals until phase-separation occurred.

Analysis of SAXS data

Calibration of the scattering intensity, $I(q)$, coming from the aggregates in the sample solutions was carried out using the following equation

$$I(q) = \frac{I_{\mathrm{sol}}(q)}{C_{\mathrm{sol}}T_{\mathrm{sol}}} - \frac{I_{\mathrm{solv}}(q)}{C_{\mathrm{solv}}T_{\mathrm{solv}}} \quad , \tag{1}$$

where $q = 4\pi \sin\theta/\lambda$ and $I_{\mathrm{sol}}(q)$, $I_{\mathrm{solv}}(q)$, C_{sol}, C_{solv}, T_{sol}, T_{solv}, 2θ and λ denote the scattering intensities of the solution and pure solvent, the incident X-ray beam intensities for the solution and for the solvent, the X-ray beam transmissions through the sample, the scattering angle and the incident wavelength, respectively. The T values were estimated by using the X-ray mass absorption coefficients of the elements in the samples.

At low angles, the X-ray scattering data were analyzed using Guinier's law,

$$I(q) = I(0)\exp\left(\frac{-q^2R_g^2}{3}\right) \quad , \tag{2}$$

where $I(0)$ is the zero-angle scattering intensity and R_g is the radius of gyration. In order to determine R_g values and $I(0)$ intensities, we used the least-squares method for the Guinier plot, $\ln I(q)$ versus q^2.

The average structures of fractals, which are generated in many growth processes of polymeric and colloidal systems, are quantitatively described using the following fractal dimension [29]:

$$M \propto R^{D_f} \quad , \tag{3}$$

where M is the mass of the fractal object, R is a measure of the radius and D_f is the fractal dimension. For surface fractals [29], the fractal structures are defined by the relationship

$$S \propto R^{D_s} \quad , \tag{4}$$

where S is the surface area and D_s is the surface fractal dimension.

Fractal structures can be characterized by SAXS techniques [29]. The profile of scattering intensity has a power-law dependence, where the exponent is simply the dimension of the mass fractals:

$$I(q) \propto q^{-D_f}, \quad 1 \leq D_f \leq 3 \quad . \tag{5}$$

The scattering curve of mass fractals provides a straight line with a slope, D_f (on a log–log plot), in the range -1 to -3, while the slopes of the scattering curve coming from surface fractals are in the range -3 to -4.

Results

The time dependence of the phase behavior for the PFOS–ethanol–1M HCl · H_2O (1:1:0.4 weight ratio) and OTMS–ethanol–1M HCl · H_2O (1:1:0.3 weight ratio) systems was examined visually. For the PFOS–ethanol–1M HCl · H_2O system, a transparent one-phase solution was obtained 35 s after mixing the sample. Two hours later, this transparent solution changed into a two-phase solution. The ^1H NMR spectra (not shown) provided evidence that the upper transparent layer and the bottom viscous, turbid layer are solvent-rich and polymer-rich, respectively. For the OTMS–ethanol–1M HCl · H_2O system, it was confirmed that phase-separation occurred after 1.5 h. Time-resolved SAXS measurements for these two sample systems were carried out until phase-separation occurred. The solvents remaining in the polymer-rich layer were removed by evaporation and the size distribution of the polymerized products was examined by GPC.

Time-resolved SAXS curves of the PFOS and OTMS systems

The time-resolved SAXS curves obtained from the transparent solution of the PFOS–ethanol–1M HCl · H_2O system are shown in Fig. 1A. The SAXS profiles depend strongly upon reaction time, showing that the extent of the formation of the PFOS polymeric precursors which result from the condensation reaction changes over time. In the initial stage of the reaction, the SAXS profile is characteristic of fractal polymer aggregates; however, the intensity of each profile in the lower q range increases with time, until finally the SAXS profile of the transparent layer becomes characteristic of that of a gel [30–32], indicating that this reaction process brings about the so-called sol–gel transition.

For analysis of the scattering curve in the intermediate region, the boundary limits $qR_g \gg 1 \gg qa$, where a is a typical chemical bond distance, are imposed on the region, and power-law behavior, which is independent of both R_g and a is predicted [33]. For a two-phase system

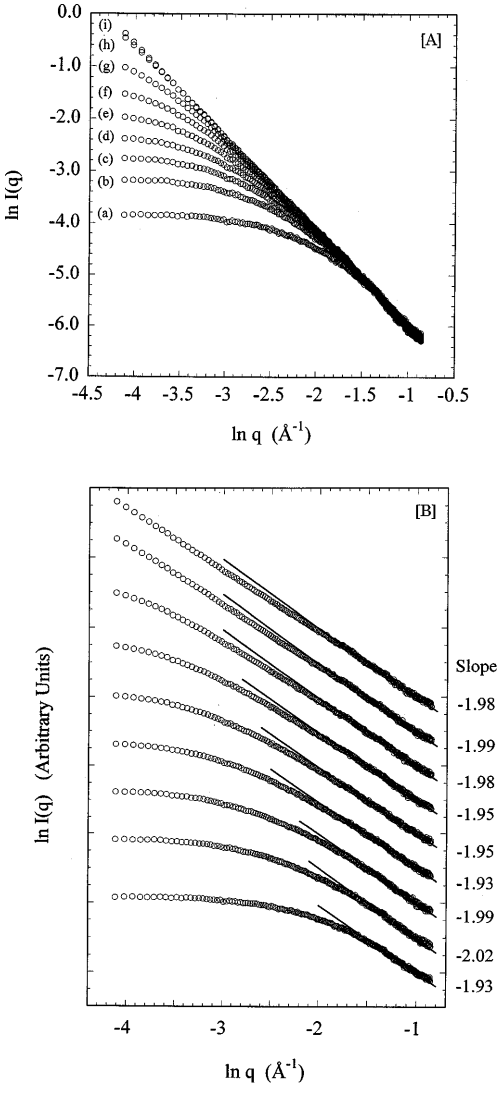

Fig. 1 **A** Time-resolved small-angle X-ray scattering curves and **B** separated spectra showing slopes of the linear region [(*a*) 500 s, (*b*) 1300 s, (*c*) 2100 s, (*d*) 2900 s, (*e*) 3700 s, (*f*) 4600 s, (*g*) 5400 s, (*h*) 6300 s, and (*i*) 7100 s] for the acid-catalyzed perfluorooctyltrimethoxysilane (*PFOS*)–ethanol system

with distinct boundaries, for example, Porod [34] has shown that the scattering curve varies as q^{-4}. For a random-walk polymer, in contrast, it should vary as q^{-2} [35]. In this present study, after taking into account both the size of the polymeric precursor (R_g) and the typical chemical bond distance ($a \simeq 3$ Å), we have assumed that the Porod regime is in the 0.166–0.333 Å^{-1} region. It should be noted that the slopes of the linear portion drawn for each profile in the intermediate region are independent of the time and are almost constant (Fig. 1B). Evidently, these scattering curves arise from polymeric precursors of PFOS (i.e. mass fractals with fractal dimension $D_f = 2$) formed by the condensation

reaction, since mass fractals will yield scattering curves with slopes between −1 and −3 [29].

The kinetics of the growth process for the PFOS polymeric precursors was examined by analyzing the time-resolved scattering curves with Guinier's law. Guinier plots, ln $I(q)$ versus q^2, of the reaction system are shown in Fig. 2. In the initial stage of the reaction, Guinier plots provide excellent linearity, but in the second stage they tend to become concave, in a manner similar to that seen in the Guinier plot for the scattering curves obtained during the base-catalyzed gelation of TEOS [12]. The time-dependence of the apparent radius of gyration (R_g) of the largest precursors in the reaction mixture is shown in Fig. 3, and the R_g values are listed in Table 1.

Between 500 and 3700 s after addition of 1M $HCl \cdot H_2O$, the apparent R_g value for the largest precursors grew from 11.1 to 34.3 Å; however, a rapid increase in R_g occurred in the reaction process after 4000 s, until finally the R_g value reached 81.7 Å at 6300 s and over 80 Å immediately before the phase-separation. These values indicate that in the initial stages of the reaction formation of small PFOS clusters occurs, while in the later stages formation of larger polymeric precursors takes place.

Time-resolved SAXS measurements for the OTMS–ethanol–1M $HCl \cdot H_2O$ system were also carried out. Time-resolved SAXS profiles, similar to those obtained for the PFOS system, were observed (profiles not shown) and a scattering profile which was characteristic of a gel with a fractal dimension of 1.7 was eventually obtained. The fractal dimension of 1.7 indicates that the reaction process for the OTMS system also involves mass fractal precursors; however, power-law analysis of the time-resolved SAXS curves (with exclusion of the datum after 4000 s) was not possible in this OTMS system, since the weak intensities of their scattering curves in the high q range make it difficult to cancel out the background intensities of the solvent.

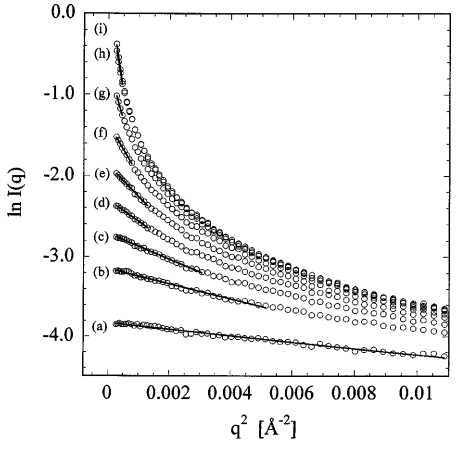

Fig. 2 Guinier plots for the acid-catalyzed PFOS–ethanol system: (*a*) 500 s, (*b*) 1300 s, (*c*) 2100 s, (*d*) 2900 s, (*e*) 3700 s, (*f*) 4600 s, (*g*) 5400 s, (*h*) 6300 s, and (*i*) 7100 s

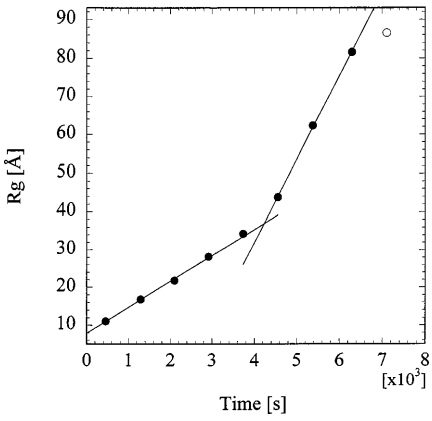

Fig. 3 Radius of gyration (R_g) versus time for the acid-catalyzed PFOS–ethanol system (○: phase-separation occurred at this point)

Table 1 Time-dependence of R_g for the perfluorooctyltrimethoxysilane (*PFOS*) and *n*-octyltrimethyoxysilane (*OTMS*) systems

	Time (s)	R_g (Å)
PFOS		
	500	11.1
	1300	16.8
	2100	21.8
	2900	28.2
	3700	34.4
	4600	43.9
	5400	62.4
	6300	81.7
	7100[a]	86.6
OTMS		
	640	11.8
	1500	18.6
	2300	27.7
	3100	47.7
	4100	83.3

[a] Phase-separation started at 7100 s

Guinier plots of the OTMS system are shown in Fig. 4. The R_g values obtained are also listed in Table 1. It is found that the time-dependent features of the Guinier plots are very similar to those seen in the PFOS system and, as in the PFOS system, growth of the OTMS precursors occurs in two stages on a short time scale after addition of 1M HCl as catalyst (Fig. 5).

Size distribution of PFOS and OTMS precursors

In order to confirm the size distribution of the polymeric precursors, we used GPC to measure the molecular size distribution of samples which were obtained after phase-separation. The number-average molecular weight (M_n)

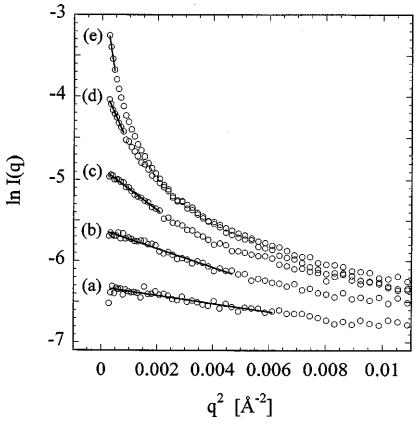

Fig. 4 Guinier plots for the acid-catalyzed *n*-octyltrimethoxysilane (*OTMS*)–ethanol system: (*a*) 640 s, (*b*) 1500 s, (*c*) 2300 s, (*d*) 3100 s, (*e*) 4100 s

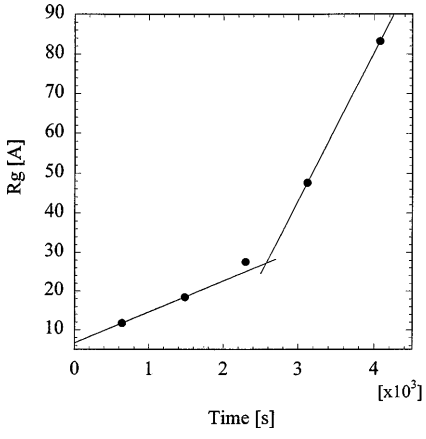

Fig. 5 Radius of gyration (R_g) versus time for the acid-catalyzed OTMS–ethanol system

and the weight-average molecular weight (M_w) for the gel samples of OTMS were 2068 (average degree of polymerization = 10.9) and 4654 (average degree of polymerization = 24.6), respectively. The ratio of M_w/M_n was 2.25, showing the polydispersity of these molecules. Figure 6 (line a) shows the distribution of molecular size for the OTMS polymer-rich sample. We note that the distribution of the molecular size extends over a wide range of molecular weight from very low (373) to very high (36 983). It should be emphasized that there exists a distribution of polymeric precursors with small size and that the distribution of precursors of larger size extends exponentially into the high-molecular-weight range.

Given the extensive distribution in size of small OTMS polymeric clusters, we may assume that this variation depends on time, as described later. In the initial stages of the reaction, it is likely that polymeric clusters of small size are predominant; however, as the

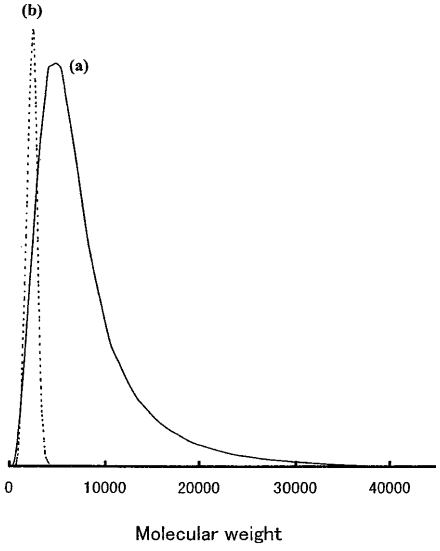

Fig. 6 Gel permeation chromatography mass distribution for polymeric precursors of PFOS (*broken line*) and of OTMS (*solid line*) obtained after phase-separation

reaction proceeds further, the population of small precursors decreases while that of larger precursors increases, until the molecular size distribution in the system eventually reaches that shown in Fig. 6(line a).

For the sample of PFOS, which was obtained from the polymer-rich layer after phase-separation, the M_n and M_w values were 1949 (average degree of polymerization = 4.6) and 2101 (average degree of polymerization = 5.1), respectively, and the M_w/M_n ratio was 1.08, indicating that these molecules are almost monodisperse. The size distribution of the PFOS polymeric sample is shown in Fig. 6(line b). The size distribution is now seen to be very narrow, indicating that these molecules are oligomeric.

These data for the size distribution for OTMS and PFOS samples are very useful for interpretation of the time dependence of the apparent radius of gyration.

It is well known that the formation of the silica polymers, which occurs during acid-catalyzed hydrolysis at low water and acid concentrations, is governed by the mechanism of the hydrolysis reaction and not by that of the condensation reaction [12]. In particular, the acid-catalyzed hydrolysis of TEOS or TMOS, which proceeds by a mechanism involving electrophilic attack on an alkoxide oxygen, is not sensitive to the electronic effects of the other groups bonded to silicon, but is affected by steric effects (i.e. steric restriction) [11, 12].

Thus, we may expect that the bulky perfluorooctyl or *n*-octyl hydrocarbon chain provides a marked steric effect for the acid-catalyzed hydrolysis of PFOS or OTMS. In particular, the marked difference in the size distribution between PFOS and OTMS polymeric clusters is probably a consequence of the great rigidity

of the perfluorooctyl chain compared with that of the octyl hydrocarbon chain, since the helical conformation of the perfluoro carbon chain should be largely stabilized by the steric effect of the bulky fluorine atom which will make the chains more rigid. This steric restriction would hinder large-size polymerizations of PFOS.

Discussion

Power-law analysis in the intermediate region, as carried out for the time-resolved SAXS curves of the acid-catalyzed PFOS–ethanol system, shows approximately $I(q) \propto q^{-2}$. Each time-resolved scattering curve furnishes a slope in the range −1.93 to −2.02 (Fig. 1B), showing that each scattering curve arises from a polymeric structure and not from individual particles [29].

Schaefer and Keefer [3] generated fractal clusters of silica and measured the fractal dimension ($D_f = 2$) of branched silica polymers by use of SAXS. They confirmed that the dimension is independent of the branching ratio and does not change during the course of polymerization to a gel.

The present observation that the fractal dimensions of the PFOS polymeric percursors formed during the reaction process are almost constant ($D_f = 2$) is very similar to Schaefer and Keefer's observation for silica polymers. Schaefer and Keefer [3] suggested that the fractal dimension ($D_f = 2$) observed for silica polymers is due to structures called lattice animals [36], which are randomly branched analogs of self-avoiding linear chains of $D_f = 2$. This situation may also exist for the present PFOS polymeric precursors. Thus, we may assume that the condensation reaction of PFOS in ethanol brings about formation of the mass fractal structure.

Kinetic growth models [6, 7, 29, 36], which describe the processes of polymerization and aggregation that occur far from equilibrium, have already been presented for the growth process of silica polymers. Monomer–cluster (MC) growth and cluster–cluster (CC) growth [29], which are distinguished by assumptions concerning accretion, may be modified to conform to the growth process of the PFOS polymeric precursors.

The following explanation may account for the mechanism of the growth process of the polymeric precursors in the PFOS–ethanol–1M HCl · H_2O system. In the initial step (Eq. 6), the acid-catalyzed hydrolysis of the three methoxy portions (i.e., formation of reactive monomers) commences, and subsequent formation of dimers occurs. Furthermore, reaction between monomers and dimers brings about trimers, i.e., the growth of monomers to form small clusters (i.e., MC growth) is predominant in the initial stage. In this step, reactive monomers play an important role, since the population of monomers may be high compared with that in the second step.

$$F(CF_2)_6CH_2CH_2Si(OCH_3)_3 \rightarrow F(CF_2)_6CH_2CH_2Si(OH)_3 \quad (6)$$

$$2F(CF_2)_6CH_2CH_2Si(OH_3)_3 \rightarrow F(CF_2)_6CH_2CH_2(OH)_2Si{-}O{-}Si(OH)_2CH_2CH_2(CF_2)_6F \quad (7)$$

In the second step, it is probable that a condensation reaction between small clusters (between dimers or between dimer and trimer or between larger oligomers) is predominant, leading to further growth of small clusters, i.e., CC growth is predominant in the second step.

In order to confirm the high population of monomers in the initial stage, the time-resolved ^1H NMR spectra of the PFOS–deuterated ethanol–1M HCL · H_2O system were measured. The time dependence of the ^1H signals of the $SiCH_2$ protons is shown in Fig. 7 together with

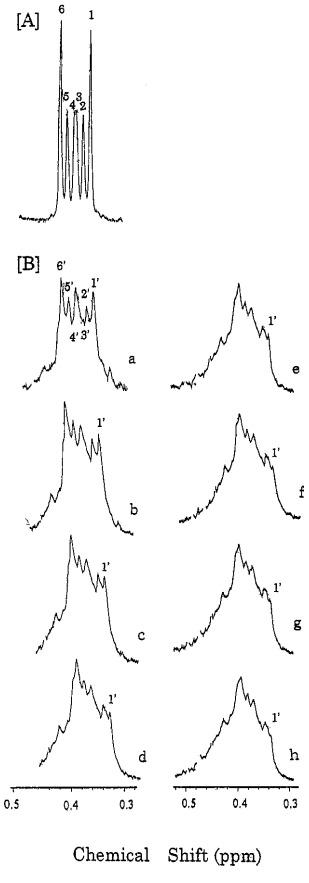

Fig. 7 **A** ^1H signals of the $SiCH_2$ protons for unhydrolyzed PFOS in deuterated ethanol and **B** the time-dependence of the ^1H signals of the $SiCH_2$ protons in the acid-catalyzed PFOS–ethanol system [initial step: (*a*) 990 s, (*b*) 1470 s, (*c*) 2400 s, (*d*) 3000 s; second step: (*e*) 4500 s, (*f*) 5100 s, (*g*) 5700 s, (*h*) 6300 s]

the ^1H signal of the $SiCH_2$ protons of unhydrolyzed PFOS. We may assume that the appearance of the ^1H signal for the $SiCH_2$ protons of the hydrolyzed PFOS monomer is very similar to that of unhydrolyzed PFOS (Fig. 7A) since spin–spin coupling (through four or five bonds) between the $SiCH_2$ and OCH_3 protons may be neglected [37]. Therefore, we can use the ^1H signals of the $SiCH_2$ protons of unhydrolyzed PFOS as an indicator of the reactive monomer.

As seen in Fig. 7B, as the reaction proceeds, the ^1H spectral appearance of the $SiCH_2$ protons changes markedly. We note that the ^1H spectral pattern obtained in the initial stages of the reaction involves relatively sharp ^1H resonance peaks (1′–6′ peaks) which closely correspond to those (1–6 peaks) for unhydrolyzed PFOS, Fig. 7A, indicating that monomers exist in the initial stage in the reaction mixture and that their population is relatively high compared with that in the second stage. It may be emphasized that, in the second stage, the peak 1′ arising from monomers decreases in intensity and broadening of other peaks occurs, until finally all the ^1H signals of the $SiCH_2$ protons become broad as a consequence of polymerization. Thus, the time-resolved ^1H NMR spectra of the $SiCH_2$ protons support the MC growth model in the initial step.

The mechanism of cluster growth in the second stage should be noted in connection with the mechanism of the sol–gel transition. Brinker et al. [12] noted the existence of polymeric structures weakly cross linked with each other in the TEOS–alcohol system. We may apply this idea to the growth process in the second stage of the PFOS or OTMS precursors, which will initially be weakly cross linked with each other, until finally, after extensive cross-linking has occurred, phase-separation into a solvent-rich upper layer and a polymer-rich bottom layer will occur.

However, we must emphasize that, in the present PFOS or OTMS system, a perfluorooctyl or octylhydrocarbon group is bonded directly to a Si atom. Although both perfluorooctyl and octylhydrocarbon chains are hydrophobic, the perfluorooctyl chain, in particular, has both hydrophobic and lipophobic properties. Therefore, for the growth process of polymeric precursors in the acid-catalyzed PFOS–ethanol or OTMS–ethanol systems, we should consider the hydrophobicity and lipophobicity of these bulky chains, in addition to the cross-link effect.

Thus, the hydrophobic interactions probably exist between clusters in the growth process, leading to the giant precursors which induce phase-separation. In fact, the very large R_g value (about 80 Å) of the PFOS polymeric precursors, which exist immediately prior to phase-separation, implies the existence of a bulky PFOS moiety. We may therefore regard these precursors as giant aggregates with a mass fractal structure, which involve self-assembling perfluorooctyl chains in their microstructure.

Unfortunately, the present SAXS data provide only the apparent radius of gyration of the aggregate and do not give us information on the detailed structure of the mass fractal formed by PFOS and OTMS. Further experiments on the concentration effect of PFOS or OTMS on the time-resolved SAXS curves and of the base-catalyzed polymerization processes are highly desirable for further discussion of the detailed structure of the mass fractal.

Conclusion

The time-resolved SAXS data for the acid-catalyzed polymerization process in the PFOS–ethanol or the OTMS–ethanol system have been analyzed using Guinier's law. We have found from the plot of R_g against reaction time that the growth of the polymeric precursors prior to phase-separation proceeds in two steps, in which formation of reactive monomers, dimers and clusters of small size occurs in the initial step, while in the second step, clusters with a larger size are formed. The time for commencement of the growth process for the second step can be regarded as a transition during which variation of the macroscopic structure occurs before onset of the macroscopic sol–gel transition.

The PFOS and OTMS polymeric precursors can also be regarded as large-scale self-assembled aggregates, whose scattering behavior should be analyzed in terms of theoretical models. In particular, theoretical analysis is essential for elucidating the effect of branching and polydispersity on the scattering behavior of these aggregates. Such a study is currently in progress and uses the theoretical model developed by Benoit [38].

References

1. Bechtold MF (1955) J Phys Chem 59:532
2. Sakka S, Kamiya K (1982) J Non-Cryst Solids 48:31
3. Schaefer DW, Keefer KD (1984) Phys Rev Lett 53:1383
4. Fricke J (May 1988) Sci Am 258:92
5. Mandelbrot BB (1982) The fractal geometry of nature. Freeman, San Francisco
6. Witten TA, Cates ME (1986) Science 232:1607
7. Sander LM (1987) Sci Am 256:94
8. Meakin P (1989) Adv Colloid Interface Sci 28:249
9. Martin JE, Hurd AJ (1987) J Appl Crystallogr 20:61

10. Schaefer DW (1988) Mater Res Soc Bull 13-2:22
11. Schaefer DW, Keefer KD (1986) Mater Res Soc Symp Proc 73:277
12. Brinker CJ, Keefer KD, Schaefer DW, Ashley CS (1982) J Non-Cryst Solids 48:47
13. Keefer KD, Schaefer DW (1986) Phys Rev Lett 56:2376
14. Keefer KD (1984) Mater Res Soc Symp Proc 32:15
15. Stellbrink J, Willner L, Jucknischke O, Richter D, Lindner P, Fetters LJ, Huan JS (1998) Macromolecules 31:4189
16. (a) Beaucage G, Schaefer D (1994) J Non-Cryst Solids 172–174:797; (b) Beaucage G (1995) J Appl Crystallogr 28:717; (c) Beaucage G (1996) J Appl Crystallogr 29:134
17. Johanson OK, Stark FO, Vogel GE, Fleischmann RM (1967) J Compos Mater 1:278
18. Kwei TK (1965) J Polym Sci A 3:3229
19. Erickson PW, Pluddmann EP (1974) In: Brautman LJ, Krock RH (eds) Composite materials, vol 6. Academic, New York, Ch 6, p 1
20. Rosen MR (1978) J Coat Technol 50:70
21. Dibenedetto AT, Nicolais L, Ambrosi L, Groeger J (1986) In: Ishida H, Koenig JL (eds) Composite interfaces. Elsevier, Amsterdam, p 47
22. Ishida H (1985) In: Ishida H, Kumar C (eds) Molecular characterization of composite interfaces. Plenum, New York, p 25
23. Lee LH (1968) J Colloid Interface Sci 27:751
24. Ishida H, Koenig JL (1978) J Colloid Interface Sci 64:555
25. Shimizu I, Okabayashi H, Taga K, Yoshino A, Nishio E, O'Connor CJ (1997) Vib Spectrosc 14:125
26. Vrancken KC, Van Der Voort P, Gillis-D'Hamers I, Vansant EF, Grobet P (1992) J Chem Soc Faraday Trans 88:3197
27. Jönsson B, Lindman B, Holmberg K, Kronberg B (1998) Surfactants and polymers in aqueous solution. Wiley, Chichester, p 31
28. Ueki T, Hiiragi E, Izumi Y, Tagawa H, Kataoka H, Muroga Y, Matsushita T, Amemiya Y (1984) Photon Factory Activity Report KEK Progress Report 83-1 KEK, Tsukuba, Japan, pp VI 70–71
29. Schaffer DW (1989) Science 243:1023
30. Daoud M, Martin JE (1989) In: Avenir D (ed) The fractal approach to heterogeneous chemistry. Wiley, New York, pp 109–130
31. Adam M, Lairez D (1996) In: Cohen Addad JP (ed) physical properties of polymeric gels. Wiley, New York, pp 87–142
32. Bouchard E, Delsanti M, Adam M, Daoud M (1986) J Phys 47:1273
33. Schaefer DW, Joany JF, Pincus P (1980) Macromolecules 13:1280
34. Porod G (1951) Kolloid-Z 83
35. de Gennes PG (1979) Scaling concepts in polymer physics. Cornell University Press, Ithaca
36. Daoud M, Family F (1984) J Phys (Paris) Lett 45:L151
37. Shimizu I, Okabayashi H, Hattori N, Taga K, Yoshino A, O'Connor CJ (1997) Colloid Polym Sci 275:293
38. Benoit H (1953) J Polym Sci 11:507